Implementable hybrid entanglement witness

Gaël Massé,[1,*] Thomas Coudreau,[1] Arne Keller,[2] and Perola Milman[1]
[1]*Université de Paris, Laboratoire Matériaux et Phénomènes Quantiques, CNRS, F-75013 Paris, France*
[2]*Université Paris-Saclay, Laboratoire Matériaux et Phénomènes Quantiques, CNRS, F-75013 Paris, France*

(Received 11 April 2020; revised 23 August 2020; accepted 23 September 2020; published 8 December 2020)

Hybrid encoding of quantum information is a promising approach towards the realization of optical quantum protocols. It combines advantages of continuous variables encoding, such as high efficiencies, with those of discrete variables, such as high fidelities. In particular, entangled hybrid states were shown to be a valuable resource for quantum information protocols. In this work we present a hybrid entanglement witness that can be implemented on available experiments and is robust to noise currently observed in quantum optical setups. The proposed witness is based on measurements of genuinely hybrid observables. The noise model we consider is general. It is formally characterized with Kraus operators since the considered hybrid system can be expressed in a finite dimension basis. A practical advantage of the witness is that it can be tested by measuring just a few experimentally available observables.

DOI: 10.1103/PhysRevA.102.062406

I. INTRODUCTION

Many different platforms are envisaged to process quantum information, corresponding to different ways of encoding qubits. All these implementations fall into two main categories: discrete variables (DVs), based on observables with discrete spectra and continuous variables (CVs), based on ones with continuous spectra. Both regimes present specific advantages and drawbacks: while DVs show high fidelities, their efficiencies are in general low and the contrary applies for CV implementations [1,2]. Hybridization between DV and CV states can take advantage of both encodings to implement certain quantum protocols [3]. An example is near deterministic teleportation with high fidelities [4–6], steering [7], Bell protocols [8–11], and hybrid quantum repeaters [12,13]. Quantum information processing using this technique is currently being developed both theoretically [14–17] and experimentally [7,18–21].

Entanglement lies at the heart of quantum physics and is a key resource for quantum information and computation [22,23]. Its detection is thus of crucial importance and has been studied extensively, notably with so-called entanglement witnesses (EW) [23]. The fact that there exist EW for every entangled state [24] has raised their importance on a theoretical point of view even further [25], and links between entanglement witness and other important features of quantum physics such as Bell inequalities have been assessed [26]. Whenever one is interested in a hybrid resource, the issue of entanglement appears naturally, since we deal with a bipartite quantum system. As a consequence, the complementarity principle will involve producing entangled states. For this reason, entanglement detection is a foundational issue in hybrid encoding.

Entanglement witnesses (EWs) have been studied extensively for discrete [27] and continuous [28] systems. Nevertheless, EWs involving measurements of observables with a continuous spectrum seem harder to establish [2]. This is particularly true if the states considered are non-Gaussian, which is precisely the case of all hybrid states [29]. The complete knowledge of the system's density matrix is a sufficient condition to compute EWs [30–35], but it is not necessary. Besides, this is not a practical solution since it requires time demanding quantum tomography techniques.

One natural way for detecting entanglement in CV systems is to use inseparability criteria based on matrices of moments [36,37], an approach subsumed in Ref. [38] and applied in Refs. [32,39–42], which can be generalized to a hybrid system [1]. Another approach was given in [33] where it was shown that the negativity volume of the generalized Wigner function can be used to detect entanglement for hybrid states. These approaches are however too sensitive to noise or too costly in terms of measurements with regard to our goals.

In this work we introduce an implementable entanglement witness for a given quantum optics setup where hybrid entangled states are currently produced experimentally [1,43]. Our approach is inspired by the well known entanglement witness [25]

$$W = \lambda \mathbb{1} - |\psi\rangle\langle\psi|, \tag{1}$$

where $\lambda \in \mathbb{R}$ is optimized such that $\mathrm{Tr}[W\sigma] > 0$ for any separable state σ and $\mathrm{Tr}[W\rho] < 0$, for the largest possible set of entangled states including $\rho = |\psi\rangle\langle\psi|$. We then adapt W so that it is robust to noise using a realistic noise model, and require the measurement of only a few observables. We choose to stick to a specific experimental setup to produce a concrete and experimentally realistic example of an efficient hybrid entanglement detection. However, the construction of

*gael.masse@univ-paris-diderot.fr

the witness enables its adaptation to other experimental platforms using different encodings, as for instance in [21], as we will show.

We begin with the study of a general noise model applied on a specific hybrid entanglement setup (Sec. II). We propose an entanglement witness, make it robust to noise, implementable, and finally present a measurement protocol (Sec. III). We sum up our work and discuss its scope in a last part (Sec. IV).

II. NOISE MODELS FOR HYBRID OPTICAL STATES

We start by introducing the family of entangled states we aim to characterize.

A. Case study on a specific encoding

We consider the experimental quantum optics setup described in detail in Ref. [43]. It is designed to produce, in the ideal scenario, the following pure state of the electromagnetic field:

$$|\psi\rangle = \frac{|0\rangle\,|C^-(\alpha)\rangle + |1\rangle\,|C^+(\alpha)\rangle}{\sqrt{2}}, \tag{2}$$

where

$$|C^\pm(\alpha)\rangle = \frac{|\alpha\rangle \pm |-\alpha\rangle}{N^\pm(\alpha)} \tag{3}$$

are the so-called symmetric and antisymmetric "Schrödinger cat"-like states, with $|\alpha\rangle \in \mathbb{C}$ being a coherent state of amplitude α, and $N^\pm(\alpha) = 2(1 \pm e^{-2|\alpha|^2}])$, so that $\langle\psi|\psi\rangle = 1$. Its specific advantage with respect to the hybrid state $\frac{|0\rangle|\alpha\rangle+|1\rangle|-\alpha\rangle}{\sqrt{2}}$, which was considered in [1,44], is that in Eq. (3) the two considered continuous variables states are orthogonal to each other for all values of α. From now on, α will be taken real, without loss of generality [43]. As for the discrete part of $|\psi\rangle$, we consider, as in Ref. [43], that $|0\rangle$ is the vacuum and $|1\rangle$ is the Fock state with one photon. However, the derivation of the witness that we present here can be adapted to other discrete encodings such as orthogonal polarization states of the photon [17,45].

In experiments, the produced state is noisy and should be described by a density matrix ρ_{noise} instead of $|\psi\rangle$. A correct modelization of ρ_{noise} depends crucially on the type of encoding as well as on the specificities of the considered experimental setup. In the present context we consider photon losses in both discrete and continuous channels as being the main source of noise. Such losses can be modeled by the action of a beam splitter (BS) [46] which entangles an ideal incoming state $|\psi\rangle\langle\psi|$ with an ancillary fluctuating quantum field. We note ρ_{da} and ρ_{ca} the ancillary fields, respectively, on the discrete channel and the continuous channel, and these beam splitters are referred to as TBS, for theoretical beam splitters, in the scheme we propose in Fig. 1. After recombination on the beam splitter, two outputs are produced corresponding to the transmitted part of the beam splitter and to the reflected one. We trace out the reflected one which corresponds to the losses, and obtain the mixed state $\rho_{\text{noise}} = \text{Tr}_{r_c,r_d}[|\psi_{\text{noise}}\rangle\langle\psi_{\text{noise}}|]$

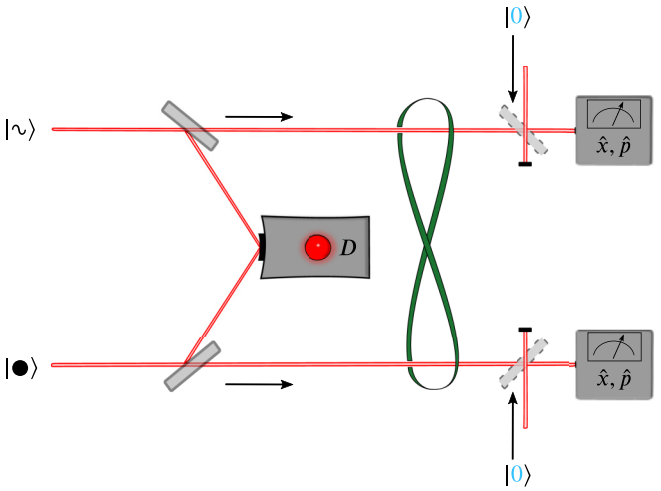

FIG. 1. Conceptual schematic for generating hybrid entanglement by deflecting a photon from either a continuous mode $|\sim\rangle$ or a discrete mode $|\bullet\rangle$ on a photon detector D. The effect of noise is modelized by mixing either modes with vacuum $|0\rangle$ on a theoretical beam splitter. The quadratures $\hat{x}$, $\hat{p}$ are measured with homodyne detectors.

with

$$\begin{aligned}|\psi_{\text{noise}}\rangle = &\frac{\left(|\sqrt{1-\eta_c}\alpha\rangle_{t_c}\,|\sqrt{\eta_c}\alpha\rangle_{r_c} - \right)|0\rangle_{t_d}\,|0\rangle_{r_d}}{\sqrt{2}N^-(\alpha)}\\ &- \frac{\left(|-\sqrt{1-\eta_c}\alpha\rangle_{t_c}\,|-\sqrt{\eta_c}\alpha\rangle_{r_c}\right)|0\rangle_{t_d}\,|0\rangle_{r_d}}{\sqrt{2}N^-(\alpha)}\\ &+ \frac{\left(|\sqrt{1-\eta_c}\alpha\rangle_{t_c}\,|\sqrt{\eta_c}\alpha\rangle_{r_c}\right)\sqrt{1-\eta_d}\,|1\rangle_{t_d}\,|0\rangle_{r_d}}{\sqrt{2}N^+(\alpha)}\\ &+ \frac{\left(|-\sqrt{1-\eta_c}\alpha\rangle_{t_c}\,|-\sqrt{\eta_c}\alpha\rangle_{r_c}\right)\sqrt{1-\eta_d}\,|1\rangle_{t_d}\,|0\rangle_{r_d}}{\sqrt{2}N^+(\alpha)}\\ &+ \frac{\left(|\sqrt{1-\eta_c}\alpha\rangle_{t_c}\,|\sqrt{\eta_c}\alpha\rangle_{r_c}\right)\sqrt{\eta_d}\,|0\rangle_{t_d}\,|1\rangle_{r_d}}{\sqrt{2}N^+(\alpha)}\\ &+ \frac{\left(|-\sqrt{1-\eta_c}\alpha\rangle_{t_c}\,|-\sqrt{\eta_c}\alpha\rangle_{r_c}\right)\sqrt{\eta_d}\,|0\rangle_{t_d}\,|1\rangle_{r_d}}{\sqrt{2}N^+(\alpha)},\end{aligned} \tag{4}$$

where Tr_{r_c,r_d} denotes the partial trace over the reflected modes, respectively, in the continuous and discrete channels, t_c and t_d are the transmitted modes, respectively, in the continuous and discrete channels and η_c^2, η_d^2 are the reflectivity of the theoretical beam splitters, respectively for the continuous channel and for the discrete channel. Therefore, η_c and $\eta_d \in [0,1]$ characterize the noise in both channels $\eta_{c/d} = 0$ being the ideal case and $\eta_{c/d} = 1$ the completely noisy channel.

The experimental setup we consider here uses optical fields at room temperature, so it is reasonable to take $\rho_{ca} = \rho_{da} = |0\rangle\langle 0|$. Indeed, for optical frequencies, the average number of thermal photon at room temperature is $\langle n\rangle = \frac{1}{e^{\frac{h\nu}{k_B T}}-1} \approx 10^{-54}$. We nonetheless also considered the case where the fluctuating ancillary fields ρ_{da} and ρ_{ca} are thermal fields at finite

temperature instead of vacuum, as shown in Appendix A. It does not change our results qualitatively.

An important aspect of the noise model we considered is that it does not increase the dimension of the pure state. Indeed, ρ_{noise} can be represented as a 4×4 matrix like the original $|\psi\rangle\langle\psi|$, albeit in a different basis. The complete expression of ρ_{noise} after performing the partial trace is given in Appendix B. It is a "mixed hybrid entangled states," according to the classification of Kreis and van Loock in their seminal works [29,47]. Consequently, its entanglement can be studied analogously to a DV only system: one can define a subspace dependent Pauli-like algebra involving observables with a continuous spectrum in order to define an easy-to-implement EW.

In order to simplify the expression of the noisy state, it is convenient to write it in the following orthonormal basis:

$$\{|C^+(\sqrt{1-\eta_c}\alpha)\rangle|0\rangle, |C^+(\sqrt{1-\eta_c}\alpha)\rangle|1\rangle, \tag{5}$$

$$|C^-(\sqrt{1-\eta_c}\alpha)\rangle|0\rangle, |C^-(\sqrt{1-\eta_c}\alpha)\rangle|1\rangle\}. \tag{6}$$

In this basis, ρ_{noise} takes the following simple form:

$$\rho_{\text{noise}} = \begin{pmatrix} w & 0 & 0 & z \\ 0 & x_1 & c & 0 \\ 0 & c & x_2 & 0 \\ z & 0 & 0 & y \end{pmatrix}, \tag{7}$$

where w, z, x_1, f, x_2, z, and y are functions of η_c, η_d, and α, that are given in Appendix B.

B. Characterization of noise with Kraus operators

Another interesting aspect of being able to express the noisy state as a 4×4 system is that the photon loss noise model can be formulated as a quantum channel in terms of Kraus operators. For such, we write $\mathscr{U}(\eta_c)$ the operator performing the change of basis from $\{|C^{\pm}(\alpha)\rangle\}$ to the noise dependent basis $\{|C^{\pm}(\eta_c\alpha)\rangle\}$, for the continuous part. Then the state ρ_{noise} given by Eq. (7) can be obtained from the ideal state $|\psi\rangle\langle\psi|$, with the help of local Kraus operators $\mathscr{C}_i(\eta_c,\alpha)\mathscr{U}(\eta_c)\otimes\mathscr{D}_j(\eta_d)(i,j=1,2)$ as

$$\rho_{\text{noise}} = \sum_{i,j=1}^{2} \mathscr{C}_i(\eta_c,\alpha)\mathscr{U}(\eta_c)\otimes\mathscr{D}_j(\eta_d)|\psi\rangle \times \langle\psi|[\mathscr{C}_i(\eta_c,\alpha)\mathscr{U}(\alpha)]^\dagger\otimes\mathscr{D}_j^\dagger(\eta_d), \tag{8}$$

where the operators $(\mathscr{C}_i)$ and $(\mathscr{D}_j)$ are calculated in Appendix D. For the discrete part we obtain

$$\mathscr{D}_1 = \begin{pmatrix} 1 & 0 \\ 0 & \sqrt{1-\eta_d} \end{pmatrix}, \quad \mathscr{D}_2 = \begin{pmatrix} 0 & \sqrt{\eta_d} \\ 0 & 0 \end{pmatrix}, \tag{9}$$

which is an amplitude damping channel. The Kraus operators for the continuous part can be written as

$$\mathscr{C}_1 = \begin{pmatrix} \cos\gamma & 0 \\ 0 & \cos\delta \end{pmatrix}, \quad \mathscr{C}_2 = \begin{pmatrix} 0 & \sin\delta \\ \sin\gamma & 0 \end{pmatrix}, \tag{10}$$

with

$$\gamma = \arccos\frac{\sqrt{\{1+\exp[-2(1-\eta_c)\alpha^2]\}[1+\exp(-2\eta_c\alpha^2)]}}{\sqrt{2+2\exp(-2\alpha^2)}}$$

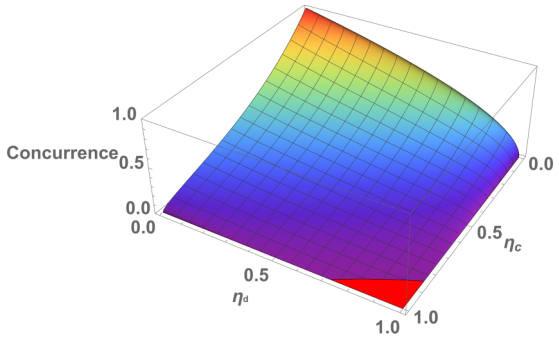

FIG. 2. Concurrence $C(\rho_{\text{noise}})$ as a function of noise parameters η_c and η_d for an amplitude $\alpha = 1$. The negative values are clipped, only the positive values indicating entanglement of ρ_{noise} are plotted (in rainbow colors).

and

$$\delta = \arccos\frac{\sqrt{\{1-\exp[-2(1-\eta_c)\alpha^2]\}[1+\exp(-2\eta_c\alpha^2)]}}{\sqrt{2-2\exp(-2\alpha^2)}}.$$

When $\gamma = \delta$ we obtain a dephasing channel, whereas when $\delta = 0$ we have an amplitude-damping channel [48], so for the continuous part, aside from the unitary transformation $\mathscr{U}$, the quantum channel is a combination of these two channels.

An alternative encoding of DV quantum information for the discrete part of our hybrid state would use the polarization degrees of freedom instead of the vacuum and one photon Fock state. In this case, the noise model would change, and it would be reasonable to consider instead a depolarizing channel on the discrete side. We can show that even in this case, the density matrix has the same form as the one presented in Eq. (7).

C. Effect of noise on entanglement

As we have noted previously, for a given value of η_c and η_d, the state ρ_{noise} can be described by a 4×4 density matrix in an orthonormal basis which depends on the noise parameter η_c. This means that we can consider it as an effective 4×4 DV system and completely characterize its entanglement [47,49,50]. To this end, we choose the concurrence C of ρ_{noise}, which takes the following simple form [51]:

$$C(\rho_{\text{noise}}) = \max(0, 2c - 2\sqrt{wy}) \tag{11}$$

(see Appendix B). For a 2-qubit system, as it is the case here, it is positive if and only if the state is entangled.

We show in Figs. 2 and 3 the variation of the concurrence $C(\rho_{\text{noise}})$ as a function of noise parameters η_c and η_d and the amplitude α. Figure 2 shows that the concurrence is decreasing with respect to the amount of noise on each channel. With $\alpha = 1$, the state ceases to be entangled only for $\eta_c = \eta_d \geqslant 0.8$, i.e., noise values well above what is actually obtained in the laboratory. Now, if we set $\eta_c = \eta_d = \eta$, we observe in Fig. 3 that the concurrence decreases with respect to α and η. Besides, the entanglement of the state becomes more and more sensitive to noise, as the amplitude α increases.

However, we do not need a full quantification of entanglement, but merely to detect its existence; besides, we want to do with the minimum number of measurements.

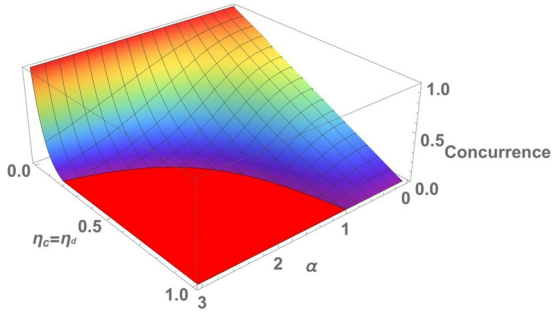

FIG. 3. Concurrence $C(\rho_{\text{noise}})$ as a function of the cat size α and the noise $\eta_c = \eta_d$. The negative values are clipped, only the positive values indicating entanglement of ρ_{noise} are plotted (in rainbow colors).

III. ENTANGLEMENT WITNESS

We now consider the entanglement witness $W = \frac{1}{2}\mathbb{1} - |\psi\rangle\langle\psi|$. $\text{Tr}[W\sigma]$ is positive for all separable state since the Schmidt rank of $|\psi\rangle$ cannot exceed 2. This is due to the fact that the Schmidt rank is bounded by the Hilbert space with the lowest dimension value: the one of the qubit. W is well suited to detect the target state $|\psi\rangle$ since $\langle\psi|W|\psi\rangle = -\frac{1}{2} < 0$.

A. Noise robustness

The relevance and usefulness of W is related to its ability to detect entanglement for a large set of ρ_{noise} states. We compute $\text{Tr}[W\rho_{\text{noise}}]$ and obtain

$$\text{Tr}[W\rho_{\text{noise}}] = \omega + y - 2c. \tag{12}$$

We show in Figs. 4 and 5 the variation of $-\text{Tr}[W\rho_{\text{noise}}]$ as a function of noise parameters η_c and η_d and the amplitude α of the cat state. The sign has been changed just to make the comparison with the concurrence easier. Figure 4 shows that W detects entanglement even when $\eta_c = \eta_d = 0.52$ for $\alpha = 1$. Since state-of-the-art optical setups can provide states with less than 20% of noise on each channel [7], we consider that the robustness is satisfying. We can now discuss the witness implementation. By comparing Fig. 5 with Fig. 3, we see that

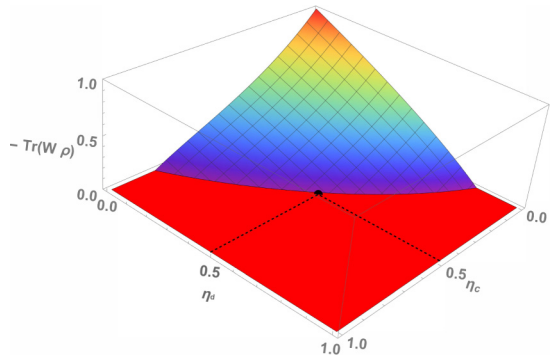

FIG. 4. $-\text{Tr}[W\rho_{\text{noise}}]$ as a function of the noise parameters η_c and η_d for a cat size $\alpha = 1$. The negative values are clipped, only the positive values indicating entanglement of ρ_{noise} are plotted (in rainbow colors). We highlight a particular point at the frontier of the detection area (coordinates $\eta_c = \eta_d = 0.52$).

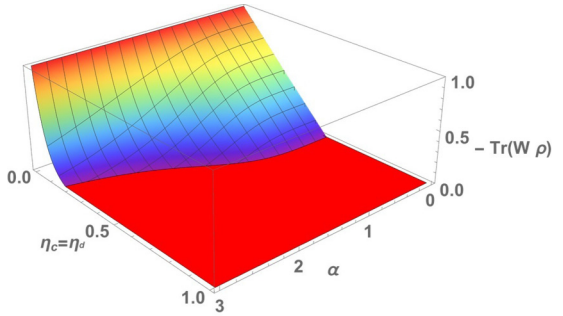

FIG. 5. $-\text{Tr}[W\rho_{\text{noise}}]$ as a function of the cat size α and the noise $\eta_c = \eta_d$. The negative values are clipped, only the positive values indicating entanglement of ρ_{noise} are plotted (in rainbow colors).

for increasing α, the region of nondetected entangled states in the form of (3) decreases: the witness tends more and more to become a necessary condition, i.e., $\text{Tr}[W\rho_{\text{noise}}] \leqslant 0 \iff C(\rho_{\text{noise}}) \geqslant 0$. Mathematically, it corresponds to the fact that $\omega \to y$ when $\alpha \to \infty$, with the notations of Eq. (7).

B. Switching to experimentally measurable observables

Measuring W involves defining local projectors characterizing $|\psi\rangle\langle\psi|$ both on its discrete and its continuous parts. For the discrete part, we can safely consider the Pauli matrices $\sigma_z = |0\rangle\langle 0| - |1\rangle\langle 1|$, $\sigma_x = |0\rangle\langle 0| + |1\rangle\langle 1|$, and $\sigma_y = \frac{1}{2i}[\sigma_z, \sigma_x]$. For the continuous part, we can define analogous observables with a continuous spectrum, i.e., with the same matrix but in the $\{|C^-(1-\eta_c)\alpha)\rangle, |C^+(1-\eta_c)\alpha)\rangle\}$ basis. Specifically,

$$\begin{aligned} X_C = {} & |C^-(1-\eta_c)\alpha)\rangle\langle C^+(1-\eta_c)\alpha| \\ & + |C^+(1-\eta_c)\alpha)\rangle\langle C^-(1-\eta_c)\alpha)|, \end{aligned} \tag{13}$$

$$\begin{aligned} Z_C = {} & |C^-(1-\eta_c)\alpha\rangle\langle C^+(1-\eta_c)\alpha| \\ & + |C^+(1-\eta_c)\alpha\rangle\langle C^-(1-\eta_c)\alpha|, \end{aligned} \tag{14}$$

$$Y_C = \frac{1}{2i}[Z_C, X_C]. \tag{15}$$

This yields

$$4|\psi\rangle\langle\psi| = [\mathbb{1} + \sigma_x \otimes X_C - \sigma_y \otimes Y_C + \sigma_z \otimes Z_C]. \tag{16}$$

Observables X_C, Y_C, and Z_C are non-Gaussian and cannot be experimentally measured in a straightforward way. In order to propose an easy way to measure the witness, we can replace them by observables that reproduce a Pauli algebra in the specific subspace of interest, that of states given in Eq. (3). Accordingly, we replace the operators X_C, Y_C, and Z_C as follows:

$$X_C \longrightarrow \frac{a + a^\dagger}{n_x}, \quad Y_C \longrightarrow \frac{i(a - a^\dagger)}{n_y}, \tag{17}$$

$$Z_C \longrightarrow \lambda_z a^\dagger a + \mu_z, \tag{18}$$

where n_x, n_y, μ_z, λ_z are normalization factors depending weakly on the parameters α, η_c, η_d of the experiment. Such observables correspond to homodyne measurements at fixed

angles. Hence, we define a new operator

$$\tilde{W} = \mathbb{1} - \frac{1}{2}\left[\mathbb{1} + \sigma_x \otimes \frac{a + a^\dagger}{n_x} - \sigma_y \otimes \frac{i(a - a^\dagger)}{n_y}\right], \quad (19)$$

which is now written in terms of observables which are currently measured in quantum optics experiments using homodyne detection [1,7,52]. $\tilde{W}$ is only an approximation of W, so we have to make sure that it is also a witness. We initially chose n_x and n_y so that W and $\tilde{W}$ coincide exactly in the subspace generated by the states of Eq. (6), but this is not a necessary condition for $\tilde{W}$ to be a witness. We present in Appendix C the calculations by which the values of n_x and n_y are optimized with regards to our objectives. Note that the term $\sigma_z \otimes Z_C$ has been discarded since it does not significantly change the value of $\mathrm{Tr}[W\rho_{\mathrm{noise}}]$ and thus does not help to detect the entanglement of ρ_{noise}. As a matter of fact, it increases the difficulty to fulfill the condition $\mathrm{Tr}[\tilde{W}\sigma] \geqslant 0$ for all σ separable.

C. Control of the new witness

We calculate in Appendix C an upper bound of the expectation value of $\tilde{W}$ for separable states. It depends on the number of photons in the continuous channel and the noise parameters η_c and η_d. The proof involves approximating the Hilbert space of the continuous part of the hybrid state by a finite dimensional Hilbert space spanned by the Fock states $\{|n\rangle ; \widehat{N}|n\rangle = n|n\rangle \text{ and } n \leqslant N\}$ where $\widehat{N}$ is the photon number operator. The value of the considered cut-off N must of course increase when the cat size α increases, but this will have an impact on the ability of the witness to detect entanglement. Therefore, a balance must be found between the parameters α, η_c, η_d in order to detect the entanglement of ρ_{noise}.

The detection of entanglement can now be carried out according to the following procedures: we choose a cut-off N, compute n_x and n_y such that no separable states within the sub-Hilbert space can violate the upper bound of the witness, and consider that the states we produce are in this subspace. This method is easy to test experimentally but overevaluates the upper bound for separable states, as detailed in Appendix C, and necessitates the assumption that the states produced experimentally have no components on the Fock states $|n\rangle$ for $n \geqslant N$.

We propose a second method which requires additional measurements but does not necessitate us to make this assumption, and that is more accurate with respect to the upper bound of the separable states. We explain it briefly here and more precisely in Appendix E. We use the method described in [53] to estimate the photon number distribution of the experimental states on the continuous channel. Using an heterodyne detection (i.e.m two conjugate homodyne detectors) on this channel, we are able to measure simultaneously two noisy orthogonal quadratures of the electromagnetic field. The sum of the square of these two output approximates sufficiently well the photon number operator $\widehat{N}$ to obtain the photon number distribution with a very good precision. Thanks to this knowledge, we are able to determine precisely the cut-off N of the continuous channel without assumptions *a priori*, and to compute an upper bound on the separable states more precise than the one obtained by method 1.

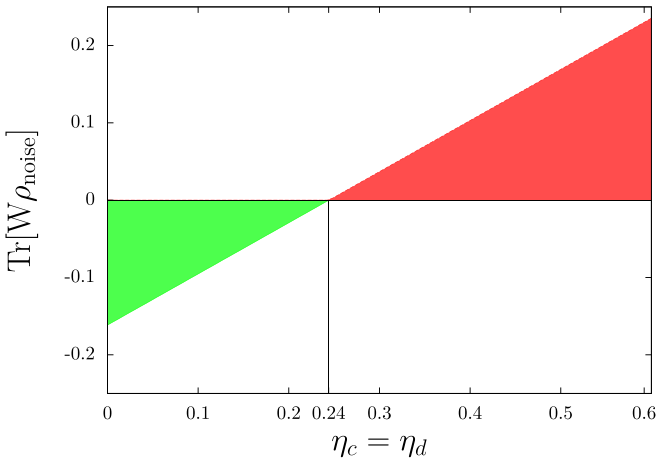

FIG. 6. $\mathrm{Tr}[\tilde{W}\rho_{\mathrm{noise}}]$ as a function of the noise parameters $\eta_c = \eta_d$ (same on both modes), with $\alpha = 1$ and cutoff at $N = 3$. Entanglement is detected in the green zone, undetected in the red zone. $\eta_{\mathrm{crit}} = 0.24$.

Finally, we also give in Appendix E, for experimental purposes, an alternative protocol for method 2 which necessitates only one homodyne detector for the continuous channel but at the expense of the accuracy in the photon number distribution estimation.

In summary, the first method uses only one homodyne for the continuous channel, but necessitates to make assumptions on the dimension of the Hilbert space. In contrast, the second method does not necessitate any assumption, thanks to its evaluation of the photon statistic. However, it requires two conjugate homodyne detectors to be fully efficient, and consequently more robust to noise.

We illustrate method 1 with two plots. Figure 6 shows the evolution of $\mathrm{Tr}[\tilde{W}\rho_{\mathrm{noise}}]$ as a function of the noise parameters $\eta_c = \eta_d$, with $\alpha = 1$ and a cutoff at $N = 3$. We see that the critical η parameter η_{crit} is equal to 24%. We plot in Fig. 7

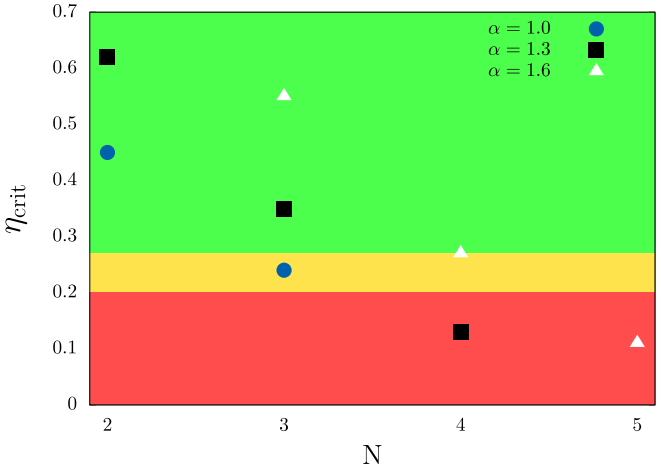

FIG. 7. Critical percentage of noise vs cutoff in the Fock space. The gold band corresponds to typical values of noise observed in state-of-the-art experiments [54]. Green zone shows a zone where the detection is experimentally easy. Red zone shows values of noise harder to obtain. $\eta_{\mathrm{crit}} = 0$ corresponds to an ideal case.

η_{crit} against N for $\alpha = 1$, $\alpha = 1.3$, and $\alpha = 1.6$ to show the sensibility of η_{crit} to N and α. Method 2 is intended to be used on experiments. In order to test its relevance, we simulated experiments, like in part IV of [53], with very good precision in the photon number distribution, that showed we could obtain $\eta_{\text{crit}} \approx 20\%$ for $\alpha = 1$, which is reasonable.

IV. SUMMARY

In this work we considered the detection of a useful entangled state currently experimentally produced in quantum optics experiments. Our entanglement witness requires, to be evaluated, only the measurements of correlations between two Pauli matrices on the discrete side, and two quadratures of the field on the continuous side. Hence, contrary to the detection of a Wigner function or even of its negativity [33], we do not need to measure displacement operators, nor do we need to use photon number resolving (PNR) detectors [55,56]. The proposed witness can be measured using homodyne detectors on both sides, discrete and continuous. This would only require us to lock the phase of the local oscillator at two angles, to obtain two orthogonal quadratures $\hat{x}$ and $\hat{p}$, whereas in a full tomography the measurement of all possible orthogonal quadratures is required. Accordingly, the protocol to detect entanglement is the following:

(1) Lock the phase of the local oscillators on the homodyne detectors to detect $\hat{x}$.

(2) Record data on both sides.

(3) Compute correlations $\langle \sigma_X \otimes \frac{a+a^\dagger}{n_x(\alpha,\eta_X)} \rangle_{\rho_{\text{expt}}}$.

(4) Lock the phase of the local oscillators on the homodyne detectors to detect $\hat{p}$.

(5) Record data on both sides.

(6) Compute correlations $\langle \sigma_Y \otimes \frac{a-a^\dagger}{n_y(\alpha,\eta_Y)} \rangle_{\rho_{\text{expt}}}$.

(7) If method 2 is chosen, compute the bound on the separable states.

(8) Compute the value of the witness.

We have presented an implementable hybrid entanglement witness that can be experimentally detected with only a few relatively easy to perform measurements. This was achieved, in a first step, by identifying observables with a continuous spectrum to Pauli matrices in a specific subspace. Such identification was possible thanks to the fact that noise, in the considered subspace, does not increase its dimension. In a second step, we replaced such observables by others, easier to measure, that coincide within the targeted subspace. We hope this work can help to understand better the subtle features of hybrid entanglement and, more generally, hybrid quantum protocols, both theoretically and experimentally.

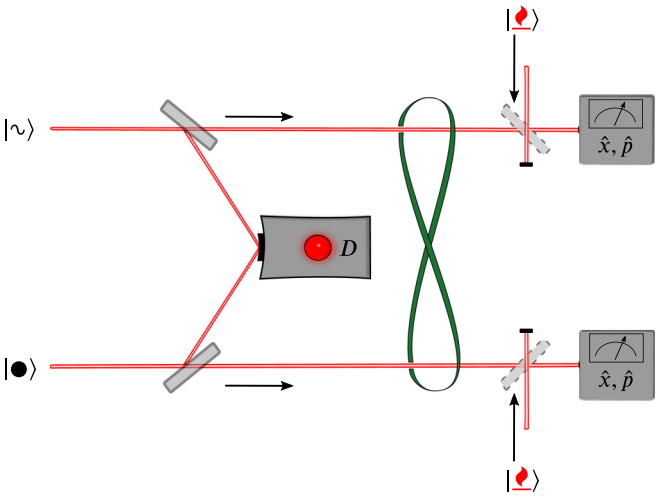

FIG. 8. Conceptual schematic for generating hybrid entanglement by deflecting a photon from either a continuous mode $|\sim\rangle$ or a discrete mode $|\bullet\rangle$ on a photon detector D. The effect of noise is modelized by mixing either modes with thermal photons $|\text{thermal}\rangle$ on a theoretical beam splitter. The quadratures $\hat{x}$, $\hat{p}$ are measured with homodyne detectors.

ACKNOWLEDGMENTS

We acknowledge fruitful discussions with T. Darras, J. Laurat, L. Garbe, and N. Fabre. G.M. acknowledges support from the French Agence Nationale de la Recherche (ANR-17-CE30-0006).

APPENDIX A: THERMAL NOISE

We study the effect of adding thermal photon noise. To do so, we replace the vacuum that we put on the beam splitter of the continuous channel by a thermal state, as featured in Fig. 8.

We derive again the value of the witness. The effect of the thermal noise on coherent states can be written, in agreement with Kreis and van Loock [29]:

$$
\begin{aligned}
\$_{\text{thermal}}(|\alpha\rangle\langle\alpha|) &= \frac{1}{2\pi\langle\text{nth}\rangle}\int_{\mathbb{C}} d^2\gamma \exp\left(\frac{-|\gamma|^2}{\langle\text{nth}\rangle}\right)|\sqrt{1-\eta_c}\alpha - \sqrt{\eta_c}\gamma\rangle\langle\sqrt{1-\eta_c}\alpha - \sqrt{\eta_c}\gamma| \\
&= \frac{1}{2\pi\langle\text{nth}\rangle}\int_{\mathbb{C}} d^2\gamma \exp\left(\frac{-|\gamma|^2}{\langle\text{nth}\rangle}\right)D(\sqrt{1-\eta_c}\alpha)|\sqrt{\eta_c}\gamma\rangle\langle\sqrt{\eta_c}\gamma|D^\dagger(\sqrt{1-\eta_c}\alpha) \\
&= \frac{1}{2\pi\langle\text{nth}\rangle}D(\sqrt{1-\eta_c}\alpha)\left[\int_{\mathbb{C}} d^2\gamma \exp\left(\frac{-|\gamma|^2}{\langle\text{nth}\rangle}\right)|\sqrt{\eta_c}\gamma\rangle\langle\sqrt{\eta_c}\gamma|\right]D^\dagger(\sqrt{1-\eta_c}\alpha) \\
&= D(\sqrt{1-\eta_c}\alpha)\$_{\text{thermal}}(|0\rangle\langle 0|)D^\dagger(\sqrt{1-\eta_c}\alpha),
\end{aligned}
$$

where D is the displacement operator such that $D(\alpha)|0\rangle = |\alpha\rangle$. From this we can compute again the value of the witness by computing the effect of the thermal noise on the cat states.

An interesting point is that the mean value of linear combinations of ladder operators with our thermal state does not depend on the temperature. *This implies that the mean value of the witness defined in Eq. (19) for our class of noisy state is the same at all temperatures*.

However, we still have to take into account thermal effects in the boundary of the value of the witness for separable state given in Appendix C. The number of photons in the continuous part can only grow, and the critical value of the maximum number of photons for which our witness is still positive for separable state would grow. The quantification of the number of additional photons is obtained through the formula $\langle n\rangle = \frac{1}{e^{\frac{h\nu}{k_B T}}-1}$.

APPENDIX B: CONCURRENCE

The expression of $\rho_{\text{full noise}}$ is in the basis formed by the kets

$$|0\rangle, |1\rangle, |\sqrt{1-\eta_c}\alpha\rangle, |-\sqrt{1-\eta_c}\alpha\rangle. \tag{B1}$$

$$\begin{aligned}
\rho_{\text{noise}} = {} & |0\rangle\langle 0|\Bigg[|\sqrt{1-\eta_c}\alpha\rangle\langle\sqrt{1-\eta_c}\alpha|\left(\frac{1}{2N^{-2}}+\frac{\eta_d}{2N^{+2}}\right)-|\sqrt{1-\eta_c}\alpha\rangle\langle-\sqrt{1-\eta_c}\alpha|\left(\frac{(\eta_d)f(\eta_c)}{2N^{+2}}+\frac{\eta_d}{2N^{-2}}\right)\\
& +|-\sqrt{1-\eta_c}\alpha\rangle\langle\sqrt{1-\eta_c}\alpha|\left(\frac{-f(\eta_c)}{2N^{-2}}+\frac{\eta_d f(\eta_c)}{2N^{-2}}\right)+|-\sqrt{1-\eta_c}\alpha\rangle\langle-\sqrt{1-\eta_c}\alpha|\left(\frac{\eta_d}{2N^{+2}}+\frac{\eta_d}{2N^{+2}}\right)\Bigg]\\
& +|1\rangle\langle 1|\Bigg[|\sqrt{1-\eta_c}\alpha\rangle\langle\sqrt{1-\eta_c}\alpha|\frac{1-\eta_d}{2N^{+2}}+|\sqrt{1-\eta_c}\alpha\rangle\langle-\sqrt{1-\eta_c}\alpha|\frac{(1-\eta_d)f(\eta_c)}{2N^{+2}}\\
& +|-\sqrt{1-\eta_c}\alpha\rangle\langle\sqrt{1-\eta_c}\alpha|\frac{(1-\eta_d)f(\eta_c)}{2N^{+2}}+|-\sqrt{1-\eta_c}\alpha\rangle\langle-\sqrt{1-\eta_c}\alpha|\frac{1-\eta_d}{2N^{+2}}\Bigg]\\
& +|0\rangle\langle 1|\Bigg[|\sqrt{1-\eta_c}\alpha\rangle\langle\sqrt{1-\eta_c}\alpha|\frac{\sqrt{1-\eta_d}}{2N^{+}N^{-}}+|\sqrt{1-\eta_c}\alpha\rangle\langle-\sqrt{1-\eta_c}\alpha|\frac{\sqrt{1-\eta_d}f(\eta_c)}{2N^{-}N^{+}}\\
& -|-\sqrt{1-\eta_c}\alpha\rangle\langle\sqrt{1-\eta_c}\alpha|\frac{\sqrt{1-\eta_d}f(\eta_c)}{2N^{+}N^{-}}-|-\sqrt{1-\eta_c}\alpha\rangle\langle-\sqrt{1-\eta_c}\alpha|\frac{\sqrt{1-\eta_d}}{2N^{+}N^{-}}\Bigg]\\
& +|1\rangle\langle 0|\Bigg[|\sqrt{1-\eta_c}\alpha\rangle\langle\sqrt{1-\eta_c}\alpha|\frac{\sqrt{1-\eta_d}}{2N^{+}N^{-}}-|\sqrt{1-\eta_c}\alpha\rangle\langle-\sqrt{1-\eta_c}\alpha|\frac{\sqrt{1-\eta_d}f(\eta_c)}{2N^{-}N^{+}}\\
& +|-\sqrt{1-\eta_c}\alpha\rangle\langle\sqrt{1-\eta_c}\alpha|\frac{\sqrt{1-\eta_d}f(\eta_c)}{2N^{+}N^{-}}-|-\sqrt{1-\eta_c}\alpha\rangle\langle-\sqrt{1-\eta_c}\alpha|\frac{\sqrt{1-\eta_d}}{2N^{+}N^{-}}\Bigg],
\end{aligned}$$

with $f(\eta_c) = \exp(-2\eta_c\alpha^2)$ and $N^{\pm} = N^{\pm}(\alpha)$ [see Eq. (3) of the main text].

If we take a specific orthonormalization, that of Eq. (6), the matrix is written

$$\rho_{\text{full noise}} = \begin{pmatrix} w & 0 & 0 & z \\ 0 & x_1 & c & 0 \\ 0 & c & x_2 & 0 \\ z & 0 & 0 & y \end{pmatrix}, \tag{B2}$$

with

$$w(\eta_c,\eta_d,\alpha) = \frac{[1+f(1-\eta_c,\alpha)]\eta_d[1+f(\eta_c,\alpha)]}{N^{+}(\alpha)^2}+\frac{[1-f(\eta_c,\alpha)]}{2N^{-}(\alpha)^2}, \tag{B3}$$

$$z(\eta_c,\eta_d,\alpha) = \frac{\sqrt{1+f(1-\eta_c,\alpha)}\sqrt{1-f(1-\eta_c,\alpha)}\sqrt{1-\eta_c}[1-f(\eta_c,\alpha)]}{N^{-}(\alpha)N^{+}(\alpha)}, \tag{B4}$$

$$x_1(\eta_c,\eta_d,\alpha) = \frac{[1+f(1-\eta_c,\alpha)](1-\eta_d)[1+f(\eta_c,\alpha)]}{2N^{+}(\alpha)^2}, \tag{B5}$$

$$x_2(\eta_c,\eta_d,\alpha) = \frac{[1-f(1-\eta_c,\alpha)][1+f(\eta_c,\alpha)]}{2N^{-}(\alpha)^2}+\frac{\eta_d[1-f(\eta_c,\alpha)]}{2N^{+}(\alpha)^2}, \tag{B6}$$

$$c(\eta_c,\eta_d,\alpha) = \frac{\sqrt{1+f(1-\eta_c,\alpha)}\sqrt{1-f(1-\eta_c,\alpha)}\sqrt{1-\eta_d}[1+f(\eta_c,\alpha)]}{2N^{-}(\alpha)N^{+}(\alpha)}, \tag{B7}$$

$$y(\eta_c,\eta_d,\alpha) = \frac{[1-f(1-\eta_c,\alpha)](1-\eta_d)[1-f(\eta_c,\alpha)]}{2N^{+}(\alpha)^2}. \tag{B8}$$

APPENDIX C: PROOF THAT $\tilde{W}$ IS A WITNESS

Let us prove that $\tilde{W}$, as defined in Eq. (19), is an entanglement witness:

$$\tilde{W} = \mathbb{1} - \frac{1}{2}\left[\mathbb{1} + X_D \otimes \frac{a + a^\dagger}{n_x} - Y_D \otimes \frac{i(a - a^\dagger)}{n_y}\right]. \quad \text{(C1)}$$

We need to check that

$$\tilde{W}_\sigma \geqslant 0 \; \forall \, \sigma \text{ separable}. \quad \text{(C2)}$$

This is equivalent to proving that

$$\left\langle X_D \otimes \frac{a + a^\dagger}{n_x} - Y_D \otimes \frac{i(a - a^\dagger)}{n_y} \right\rangle_\sigma \leqslant 1 \quad \forall \, \sigma \text{ separable}. \quad \text{(C3)}$$

The most general separable state can be written

$$\sigma = \sum_k \lambda_k \sigma_D \otimes \sigma_C, \quad \text{(C4)}$$

with $\{\lambda_k\}$ being a convex set, σ_D is a 2×2 matrix, and σ_C a $N \times N$ matrix that features the continuous part of the state, N being the cutoff of the Hilbert space of the continuous part.

We present the proof of Eq. (C3) with a pure state on the continuous part, the generalization to mixed states being obtained by convexity. Let

$$\tilde{\sigma} = \sigma_D \otimes |\psi\rangle\langle\psi|, \quad \text{(C5)}$$

with

$$|\psi\rangle = \sum_{i=0}^{N} \lambda_i |i\rangle, \quad \text{(C6)}$$

with $|i\rangle$ an eigenstate of the operator $a^\dagger a$, with $\sum_{i=0}^{N} |\lambda_i|^2$. Since σ_D is a density matrix, we write it

$$\sigma_D = \begin{pmatrix} \sigma_{11} & \sigma_{12} \\ \bar{\sigma}_{12} & 1 - \sigma_{11} \end{pmatrix}, \quad \text{(C7)}$$

with $0 \leqslant \sigma_{11} \leqslant 1$ and the following inequality holds:

$$\det(\sigma_D) \geqslant 0 \iff |\sigma_{12}| \leqslant \sqrt{\sigma_{11}(1 - \sigma_{11})}. \quad \text{(C8)}$$

Now,

$$\left\langle X_D \otimes \frac{a + a^\dagger}{n_x} \right\rangle_{\tilde{\sigma}} = (\sigma_{12} + \bar{\sigma}_{12}) \left(\sum_{i=0}^{N-1} (\bar{\lambda}_i \lambda_{i+1} \sqrt{i+1} + \lambda_i \bar{\lambda}_{i+1} \sqrt{i+1}) \frac{1}{n_x} \right). \quad \text{(C9)}$$

$$\left\langle Y_D \otimes \frac{i(a - a^\dagger)}{n_y} \right\rangle_{\tilde{\sigma}} = (\sigma_{12} - \bar{\sigma}_{12}) \left(\sum_{i=0}^{N-1} (\bar{\lambda}_i \lambda_{i+1} \sqrt{i+1} - \lambda_i \bar{\lambda}_{i+1} \sqrt{i+1}) \frac{1}{n_y} \right). \quad \text{(C10)}$$

Hence,

$$\left| \left\langle X_D \otimes \frac{a + a^\dagger}{n_x} \right\rangle_{\tilde{\sigma}} - \left\langle Y_D \otimes \frac{i(a - a^\dagger)}{n_y} \right\rangle_{\tilde{\sigma}} \right| = \left| (\sigma_{12} + \bar{\sigma_{12}}) \left(\sum_{i=0}^{N-1} (\bar{\lambda}_i \lambda_{i+1} \sqrt{i+1} + \lambda_i \bar{\lambda}_{i+1} \sqrt{i+1}) \times \frac{1}{n_x} \right) \right.$$
$$\left. - \, i(\sigma_{12} - \bar{\sigma_{12}}) \left(\sum_{i=0}^{N-1} (\bar{\lambda}_i \lambda_{i+1} \sqrt{i+1} - \lambda_i \bar{\lambda}_{i+1} \sqrt{i+1}) \times \frac{1}{n_y} \right) \right| \quad \text{(C11)}$$

$$= \left| \frac{2\mathrm{Re}(\sigma_{12}) 2\mathrm{Re}(\sum_{i=0}^{N-1} (\bar{\lambda}_i \lambda_{i+1} \sqrt{i+1}))}{n_x} - \frac{2\mathrm{Im}(\sigma_{12}) 2\mathrm{Im}(\sum_{i=0}^{N-1} (\bar{\lambda}_i \lambda_{i+1} \sqrt{i+1}))}{n_y} \right| \quad \text{(C12)}$$

$$= 4|\sigma_{12}| \left| \frac{\cos(\sigma_{12}) \sum_{i=0}^{N-1} \mathrm{Re}(\bar{\lambda}_i \lambda_{i+1} \sqrt{i+1})}{n_x} - \frac{\sin(\sigma_{12}) \sum_{i=0}^{N-1} \mathrm{Im}(\bar{\lambda}_i \lambda_{i+1} \sqrt{i+1})}{n_y} \right| \quad \text{(C13)}$$

$$= 4|\sigma_{12}| \left| \frac{\cos(\sigma_{12}) \sum_{i=0}^{N-1} |\bar{\lambda}_i| |\lambda_{i+1}| \sqrt{i+1}) \cos(\theta_k)}{n_x} - \frac{\sin(\sigma_{12}) \sum_{i=0}^{N-1} |\bar{\lambda}_i| |\lambda_{i+1}| \sqrt{i+1}) \sin(\theta_k)}{n_y} \right| \quad \text{(C14)}$$

$$= 4|\sigma_{12}| \left| \sum_{i=0}^{N-1} |\bar{\lambda}_i| |\lambda_{i+1}| \sqrt{i+1}) \left(\frac{\cos(\sigma_{12}) \cos(\theta_k)}{n_x} - \frac{\sin(\sigma_{12}) \sin(\theta_k)}{n_y} \right) \right|, \quad \text{(C15)}$$

where we have used $\lambda_k = |\lambda_k| \exp i\phi_k$ and $\theta_k = \phi_{k+1} - \phi_k$. Finally,

$$\left| \left\langle X_D \otimes \frac{a + a^\dagger}{n_x} \right\rangle_{\tilde{\sigma}} - \left\langle Y_D \otimes \frac{i(a - a^\dagger)}{n_y} \right\rangle_{\tilde{\sigma}} \right| \leqslant 2 \left| \sum_{i=0}^{N-1} |\bar{\lambda}_i| |\lambda_{i+1}| \sqrt{i+1} \max\left(\frac{1}{|n_x|}, \frac{1}{|n_y|} \right) \right| \quad \text{(C16)}$$

$$\leqslant 2 \left| f(N) \max\left(\frac{1}{|n_x|}, \frac{1}{|n_y|} \right) \right| \quad \text{(C17)}$$

where we have used $\max_{\sigma_{11} \in [0;1]} \sqrt{\sigma_{11}(1 - \sigma_{11})} = \frac{1}{2}$, $|\frac{\cos(\sigma_{12}) \cos(\theta_k)}{n_x} - \frac{\sin(\sigma_{12}) \sin(\theta_k)}{n_y}| \leqslant \max(\frac{1}{|n_x|}, \frac{1}{|n_y|})$ and defined $f(N) = \sup_{\{\lambda_i\}} \sum_{i=0}^{N-1} |\lambda_i| |\bar{\lambda}_{i+1}| \sqrt{i+1}$ with the constraint that the set of λ_i is convex.

This upper bound depends on the number of photons since it is related to the truncation in the Fock basis. Now, we can either take an arbitrary cutoff and compute a worst-case scenario with an optimization problem, or we can upper bound it tightly if we possess the knowledge of the set of $\{\lambda_i\}$. The former is presented below, whereas the latter procedure, to obtain $\{\lambda_i\}$ and upper bound the terms is explained in Appendix E.

Method 1: Worst-case scenario

We write extensively the optimization problem in Eq. (C18):

$$\sum_{i=0}^{N-1} |\lambda_i||\bar{\lambda}_{i+1}|\sqrt{i+1}, \quad \sum_{i=0}^{N} |\lambda_i|^2 = 1. \tag{C18}$$

Let us write $\lambda_k = |\lambda_k| e^{i\phi_k}$. Now $\mathrm{Re}(\lambda_k \bar{\lambda}_{k+1}) = |\lambda_k||\lambda_{k+1}| \cos(\phi_k - \phi_{k+1})$. If we want to maximize this quantity, we need $\phi_k - \phi_{k+1} = 2n\pi$. This constrain can indeed be reached. Without loss of generality, we can consequently consider that the λ_k are positive reals. This hypothesis is done from now on.

If we use the formalism of Lagrange multipliers, we need to nullify the gradient of

$$\mathscr{L}(\lambda_k, \lambda) = f(\lambda_k) - \mu g(\lambda_k), \tag{C19}$$

with respect to every λ_k and μ, with

$$f(\lambda_k) = \sum_{i=0}^{N-1} |\lambda_i||\lambda_{i+1}|\sqrt{i+1},$$

$$g(\lambda_k) = 1 - \sum_{i=0}^{N} |\lambda_i|^2. \tag{C20}$$

We obtain

$$\begin{aligned} \frac{\partial \mathscr{L}}{\partial \mu} &= -\left(1 - \sum_{i=0}^{N} |\lambda_i|^2\right) = 0, \\ \forall\, j \in [1; N-1] \quad \frac{\partial \mathscr{L}}{\partial \lambda_k} &= x_{j+1}\sqrt{j+1} + x_{j-1}\sqrt{j} + 2\mu x_j = 0, \\ \frac{\partial \mathscr{L}}{\partial \lambda_0} &= x_1\sqrt{1} + 2\mu x_0 = 0, \\ \frac{\partial \mathscr{L}}{\partial \lambda_N} &= x_{N-1}\sqrt{N} + 2\mu x_N = 0. \end{aligned} \tag{C21}$$

We can recast the last three lines into the following linear problem:

$$\begin{pmatrix} 2\mu & \sqrt{1} & \cdots & \\ \sqrt{1} & 2\mu & \sqrt{2} & \cdots \\ \vdots & \ddots & \vdots & \\ \cdots & \sqrt{N-1} & 2\mu & \sqrt{N} \\ \cdots & \ldots & \sqrt{N} & 2\mu \end{pmatrix} \begin{pmatrix} x_0 \\ x_1 \\ \vdots \\ x_{N-1} \\ x_N \end{pmatrix} = 0. \tag{C22}$$

Now we have

$$M(N)\vec{x} = \vec{0}, \tag{C23}$$

where M is the matrix displayed in (C22) and $\vec{x}$ is the vector. There exists a solution for

$$\det[M(N)] = 0. \tag{C24}$$

The determinant of M, which we note d_N, follows the recurrence relation

$$d_{N+2}(\mu) = 2\mu d_{N+1}(\mu) - (N+1) d_N(\mu). \tag{C25}$$

We can recognize the recurrence relation of the Hermite polynomials. The protocol to solve the optimization problem is the following:

(1) For a given N, compute the roots of the Nth Hermite polynomials.

(2) For every root, compute the M matrix, and look for the kernel of M.

(3) Keep $\vec{x}$ for which all terms have the same sign.

(4) Normalize it using the previous Lagrangian constraint.

Since $f(N)$, even after optimization, is above 1, we will have to damp our witness to ensure it is always positive for a separable state. This, in turn, will decrease the number of entangled states that can be detected. We are able to produce a witness for experimentally interesting values; we can obtain negative values for cat states of size 1 and for which the noise η_c, η_d can go up to 0.25, provided N is not above 4.

APPENDIX D: NAIMARK EXTENSION

We give explicit calculations of the Kraus operators. We looked for expressions of U_c and U_d through

$$\rho_{\mathrm{noise}} = \mathrm{Tr}_{r_c, r_d}(U_c \otimes U_d)(\rho \otimes \mathscr{R})\left(U_c^\dagger \otimes U_d^\dagger\right), \tag{D1}$$

with $\mathscr{R}$ a reservoir at zero temperature,

$$\mathscr{R} = \begin{pmatrix} 1 & 0 & 0 & 0 \\ 0 & 0 & 0 & 0 \\ 0 & 0 & 0 & 0 \\ 0 & 0 & 0 & 0 \end{pmatrix}, \tag{D2}$$

and

$$U_{c,d} = \begin{pmatrix} e^{i\beta_1}\cos(\delta) & 0 & 0 & e^{i\beta_2}\sin(\delta) \\ 0 & e^{i\phi_1}\cos(\gamma) & e^{i\phi_2}\sin(\gamma) & 0 \\ 0 & -e^{-i\phi_2}\sin(\gamma) & e^{-i\phi_1}\cos(\gamma) & 0 \\ -e^{-i\beta_2}\sin(\delta) & 0 & 0 & e^{-i\beta_1}\cos(\delta) \end{pmatrix}, \tag{D3}$$

so that they could modelize exchange of photons between the system and the reservoirs. We recall that ρ does not live in the same exact basis than $\rho_{\text{full noise}}$ which is why our Naimark's transformation is a formal one:

$$\rho = \begin{pmatrix} 0 & 0 & 0 & 0 \\ 0 & \frac{1}{2} & \frac{1}{2} & 0 \\ 0 & \frac{1}{2} & \frac{1}{2} & 0 \\ 0 & 0 & 0 & 0 \end{pmatrix}. \tag{D4}$$

In the basis

$$|+\rangle_d|0\rangle_{r_d}, |+\rangle_d|1\rangle_{r_d}, |-\rangle_d|0\rangle_{r_d}, |-\rangle_d|1\rangle_{r_d}, \tag{D5}$$

where d stands for discrete and r_d discrete reservoir, the expression of U_d is given by the following matrix:

$$U_d = \begin{pmatrix} 1 & 0 & 0 & 0 \\ 0 & \sqrt{1-\eta_d} & \sqrt{\eta_d} & 0 \\ 0 & -\sqrt{\eta_d} & \sqrt{\eta_d} & 0 \\ 0 & 0 & 0 & 1 \end{pmatrix}. \tag{D6}$$

On the continuous side, in the basis:

$$|+\rangle_c|0\rangle_{r_c}, |+\rangle_c|1\rangle_{r_c}, |-\rangle_c|0\rangle_{r_c}, |-\rangle_c|1\rangle_{r_c}, \tag{D7}$$

where c stands for discrete and r_c continuous reservoir, the expression of U_c is given by

$$U_c = \begin{pmatrix} \frac{\sqrt{(1+K)(1+f)}}{N^+} & 0 & 0 & \frac{\sqrt{(1-K)(1-f)}}{N^+} \\ 0 & \frac{\sqrt{(1-K)(1+f)}}{N^-} & \frac{\sqrt{(1+K)(1-f)}}{N^-} & 0 \\ 0 & -\frac{\sqrt{(1+K)(1-f)}}{N^-} & \frac{\sqrt{(1-K)(1+f)}}{N^-} & 0 \\ -\frac{\sqrt{(1-K)(1-f)}}{N^+} & 0 & 0 & \frac{\sqrt{(1+K)(1+f)}}{N^+} \end{pmatrix}, \tag{D8}$$

with $K = \exp[-2(1-\eta_c)\alpha^2]$, $f = \exp(-2\eta_c\alpha^2)$. We obtain

$$\rho_{\text{continuous noise}} = \text{Tr}p_{r_c,r_d}(Uc \otimes \mathbf{1})(\rho \otimes \mathscr{R})\left(Uc^\dagger \otimes \mathbf{1}\right), \tag{D9}$$

$$\rho_{\text{discrete noise}} = \text{Tr}p_{r_c,r_d}(\mathbf{1} \otimes Ud)(\rho \otimes \mathscr{R})\left(\mathbf{1} \otimes Ud^\dagger\right), \tag{D10}$$

$$\rho_{\text{discrete noise}} = \begin{pmatrix} \frac{\eta_d}{2} & 0 & 0 & 0 \\ 0 & \frac{1-\eta_d}{2} & \frac{\sqrt{1-\eta_d}}{2} & 0 \\ 0 & \frac{\sqrt{1-\eta_d}}{2} & \frac{1}{2} & 0 \\ 0 & 0 & 0 & 1 \end{pmatrix}, \tag{D11}$$

and $\rho_{\text{continuous noise}}$ equal to ρ_{noise} defined in (7), with η_d set to 0 (the shape of the matrix does not change). We note that $\rho_{\text{discrete noise}}$ can be expressed as the convex sum of two pure states $\rho_{\text{ent}} = |\psi_{\text{ent}}\rangle\langle\psi_{\text{ent}}|$ and $\rho_{\text{sep}} = |\psi_{\text{sep}}\rangle\langle\psi_{\text{sep}}|$,

$$\rho_{\text{discrete noise}} = \frac{1+(1-\eta_d)}{2}\rho_{\text{ent}} + \frac{1-(1-\eta_d)}{2}\rho_{\text{sep}}, \tag{D12}$$

with $|\psi_{\text{ent}}\rangle = \frac{|0\rangle|-\rangle+\sqrt{(1-\eta_d)}|1\rangle|+\rangle}{\sqrt{\eta_d}}$ an entangled state, and $|\psi_{\text{sep}}\rangle = |0\rangle|+\rangle$ a separable one. The computations of the Kraus operators, from U_c and U_d, is straightforward.

APPENDIX E: CONTROL *A POSTERIORI*

We present here method 2 described briefly in the main text. It consists of obtaining the photon number distribution, and then to use this information to obtain a precise bound for the witness described in Appendix C.

1. Photon number statistics evaluation

In this section we make a brief summary of the technique presented in the article *Characterizing photon number statistics using conjugate optical homodyne detection* [53] to evaluate very precisely the photon number distribution of a given experimental state thanks to two conjugate homodyne detectors. Given these apparatus, we measure simultaneously two orthogonal quadratures of the electromagnetic field on two different modes, which have been separated by a beam splitter. We shall denote them $\widehat{X}$ and $\widehat{P}$, where

$$\widehat{X} = \frac{1}{\sqrt{2}}[\widehat{a}^\dagger \exp(i\theta) + \widehat{a}\exp(-i\theta)], \tag{E1}$$

$$\widehat{P} = \frac{i}{\sqrt{2}}[\widehat{b}^\dagger \exp(i\theta) - \widehat{b}\exp(-i\theta)]. \tag{E2}$$

θ is the phase of the local oscillator of one of the homodyne, $\widehat{a}^\dagger$ and $\widehat{a}$ are photon creation and annihilation on one mode, and $\widehat{b}^\dagger$ and $\widehat{b}$ on the other one. This allows us to form the following observable:

$$\widehat{Z} = \widehat{X}^2 + \widehat{P}^2. \tag{E3}$$

We can see it as an approximation of the photon number operator $\widehat{N}$ (remember that $\widehat{X}$ and $\widehat{P}$ are not defined on the same mode). The probability distribution function $P_Z(z)$ of this observable depends only on the diagonal terms ρ_{nn} of the density matrix, according to the equation

$$P_Z(z) = \exp(-z)\sum_{n=0}^{\infty}\frac{\rho_{nn}}{n!}z^n. \tag{E4}$$

It means that the photon number distribution can be evaluated without having to scan the phase of the LO. Given a repeated sequence of measurement of $\widehat{Z}$, we obtain $P_Z(z)$. Then, thanks to a Bayes inversion and an algorithm of maximum likelihood, we are able to infer the diagonal terms of the density matrix ρ_{nn}.

2. Precise upper bounding of the witness for separable states

This in turn allows us to upper bound Eq. (C17) and certify that our witness cannot produce false positives. The computation of Appendix C is established for pure states but the upper bounding we propose stays true in the general case of mixed states. The calculations carried out in q. (C18) involve

the terms of the sup and subdiagonal of the density matrix, but they can be bounded by the diagonal terms, according to the following expression:

$$|\rho_{i,i\pm1}| \leqslant \sqrt{|\rho_{i,i}||\rho_{i+1,i+1}|}. \tag{E5}$$

This relation is an equality in the case of pure states. If we consider a mixed state:

$$\rho = \sum_i p_i |\psi_i\rangle\langle\psi_i|, \tag{E6}$$

with

$$|\psi_i\rangle = \sum_k \lambda_{k,i}|k\rangle, \tag{E7}$$

we have

$$|\rho_{i,i+1}| = \left|\sum_k p_k \lambda_{i,k}\bar{\lambda}_{i+1,k}\right| \tag{E8}$$

$$\leqslant \sum_k |p_k \lambda_{i,k}\bar{\lambda}_{i+1,k}| \tag{E9}$$

$$= \sum_k \sqrt{p_k^2|\lambda_{i,k}|^2|\bar{\lambda}_{i+1,k}|^2} \tag{E10}$$

$$\leqslant \sqrt{\sum_k p_k|\lambda_{i,k}|^2 \sum_l p_l|\lambda_{i+1,l}|^2} \tag{E11}$$

$$= \sqrt{|\rho_{i,i}||\rho_{i+1,i+1}|}. \tag{E12}$$

The additional experimental information we measured makes it possible for us to define a tight upper bound for the separable states that does not necessitate any *prior* knowledge of the states that are produced. Note that recently a protocol has been presented to directly estimate any element of a density matrix with a heterodyne detection [57]. Our method is less generic, but simple and sufficient for our needs.

3. A protocol with only one homodyne detector

We present a simple protocol to make a rough evaluation of the photon number distribution ρ_{nn} that only necessitates one homodyne detector, and where the quadratures will not be measured jointly. We proceed in two times, recording successively the values of $\widehat{X}$, and then the values of $\widehat{P}$ for two different set of states. We give indices 1 and 2 to the values obtained for, respectively, the first set of experiments and the second. Since we can not match anymore the right value of $\widehat{X}$ to that of $\widehat{P}$, we will form

$$\langle\widehat{Z}\rangle = \langle\widehat{X}^2 + \widehat{P}^2\rangle \leqslant \left\langle \widehat{X}_1^2 + \sup_{\widehat{P}_2} \widehat{P}_2^2 \right\rangle = \langle\widehat{Z}_{\sup}\rangle. \tag{E13}$$

Hence, we do not measure $\widehat{Z}$, but with a sufficiently important number of recorded data points, we can overevaluate it. As a consequence, the photon number distribution ρ_{nn} that we finally obtain will be shifted towards the higher values. The population terms of the low n of ρ_{nn} will be underestimated, and that of the high values of n will be overestimated. Consequently, this distribution will allow us to form an upper bound on the witness. The more the experimental states produced are squeezed on one quadrature, say the $\widehat{X}$ quadrature, the less $\langle\widehat{Z}\rangle$ will be affected by the value of the other quadrature $\widehat{P}$. As a consequence, with sufficiently squeezed states $\langle\widehat{Z}_{\sup}\rangle$ will be close to $\langle\widehat{Z}\rangle$. This will allow us to improve the bound of the witness from method 1. Note that other ways to form the upper bound of Eq. (E13) can be envisaged, for instance matching the most important value of $\widehat{P}_2$ with that of $\widehat{X}_1$, and then iterate this procedure.

[1] P. van Loock, Laser Photonics Rev. **5**, 167 (2011).
[2] X. Qi and J. Hou, Quant. Info. Proc. **15**, 741 (2016).
[3] S. Takeda and A. Furusawa, APL Photonics **4**, 060902 (2019).
[4] S. Takeda, T. Mizuta, M. Fuwa, P. van Loock, and A. Furusawa, Nature (London) **500**, 315 (2013).
[5] S.-W. Lee and H. Jeong, Phys. Rev. A **87**, 022326 (2013).
[6] S. H. Lie and H. Jeong, Photonics Res. **7**, A7 (2019).
[7] A. Cavaillès, H. Le Jeannic, J. Raskop, G. Guccione, D. Markham, E. Diamanti, M. D. Shaw, V. B. Verma, S. W. Nam, and J. Laurat, Phys. Rev. Lett. **121**, 170403 (2018).
[8] J. B. Brask, N. Brunner, D. Cavalcanti, and A. Leverrier, Phys. Rev. A **85**, 042116 (2012).
[9] M. T. Quintino, M. Araújo, D. Cavalcanti, M. F. Santos, and M. T. Cunha, J. Phys. A: Math. Theor. **45**, 215308 (2012).
[10] H. Kwon and H. Jeong, Phys. Rev. A **88**, 052127 (2013).
[11] F. Tppel and M. Stobińska, J. Phys. A: Math. Theor. **48**, 075306 (2015).
[12] M. Bergmann and P. van Loock, Phys. Rev. A **99**, 032349 (2019).
[13] J. B. Brask, I. Rigas, E. S. Polzik, U. L. Andersen, and A. S. Sørensen, Phys. Rev. Lett. **105**, 160501 (2010).
[14] Y.-B. Sheng, L. Zhou, and G.-L. Long, Phys. Rev. A **88**, 022302 (2013).
[15] Y. Lim, J. Joo, T. P. Spiller, and H. Jeong, Phys. Rev. A **94**, 062337 (2016).
[16] U. L. Andersen, J. S. Neergaard-Nielsen, P. van Loock, and A. Furusawa, Nat. Phys. **11**, 713 (2015).
[17] H. Kwon and H. Jeong, Phys. Rev. A **91**, 012340 (2015).
[18] D. V. Sychev, A. E. Ulanov, E. S. Tiunov, A. A. Pushkina, A. Kuzhamuratov, V. Novikov, and A. I. Lvovsky, Nat. Commun. **9**, 1 (2018).
[19] K. Huang, H. Le Jeannic, O. Morin, T. Darras, G. Guccione, A. Cavaillès, and J. Laurat, New J. Phys. **21**, 083033 (2019).
[20] G. Guccione, T. Darras, H. Le Jeannic, V. B. Verma, S. W. Nam, A. Cavaillès, and J. Laurat, Sci. Adv. **6**, eaba4508 (2020).
[21] É. Gouzien, F. Brunel, S. Tanzilli, and V. D'Auria, Phys. Rev. A **102**, 012603 (2020).
[22] E. Chitambar and G. Gour, Rev. Mod. Phys. **91**, 025001 (2019).
[23] R. Horodecki, P. Horodecki, M. Horodecki, and K. Horodecki, Rev. Mod. Phys. **81**, 865 (2009).
[24] M. Horodecki, P. Horodecki, and R. Horodecki, Phys. Lett. A **223**, 1 (1996).
[25] D. Chruciski and G. Sarbicki, J. Phys. A: Math. Theor. **47**, 483001 (2014).

[26] P. Hyllus, O. Gühne, D. Bruß, and M. Lewenstein, Phys. Rev. A **72**, 012321 (2005).
[27] O. Gühne and G. Toth, Phys. Rep. **474**, 1 (2009).
[28] J. Sperling and W. Vogel, Phys. Rev. A **79**, 042337 (2009).
[29] K. Kreis and P. van Loock, Phys. Rev. A **85**, 032307 (2012).
[30] M. Zhang, L. Zhou, W. Zhong, and Y. B Sheng, Chin. Phys. B **28**, 010301 (2019).
[31] A. Peres, Phys. Rev. Lett. **77**, 1413 (1996).
[32] R. Simon, Phys. Rev. Lett. **84**, 2726 (2000).
[33] I. I. Arkhipov, A. Barasiński, and J. Svozilík, Sci. Rep. **8**, 16955 (2018).
[34] J. Hou and X. Qi, Phys. Rev. A **81**, 062351 (2010).
[35] Y. Guo, X. Qi, and J. Hou, Chin. Sci. Bull. **56**, 840 (2011).
[36] A. Miranowicz, M. Piani, P. Horodecki, and R. Horodecki, Phys. Rev. A **80**, 052303 (2009).
[37] O. Gittsovich, T. Moroder, A. Asadian, O. Gühne, and P. Rabl, Phys. Rev. A **91**, 022114 (2015).
[38] E. Shchukin and W. Vogel, Phys. Rev. Lett. **95**, 230502 (2005).
[39] L.-M. Duan, G. Giedke, J. I. Cirac, and P. Zoller, Phys. Rev. Lett. **84**, 2722 (2000).
[40] S. Mancini, V. Giovannetti, D. Vitali, and P. Tombesi, Phys. Rev. Lett. **88**, 120401 (2002).
[41] M. G. Raymer, A. C. Funk, B. C. Sanders, and H. de Guise, Phys. Rev. A **67**, 052104 (2003).
[42] M. Hillery and M. S. Zubairy, Phys. Rev. Lett. **96**, 050503 (2006).
[43] O. Morin, K. Huang, J. Liu, H. Le Jeannic, C. Fabre, and J. Laurat, Nat. Photonics **8**, 570 (2014).
[44] H. Jeong, A. Zavatta, M. Kang, S.-W. Lee, L. S. Costanzo, S. Grandi, T. C. Ralph, and M. Bellini, Nat. Photonics **8**, 564 (2014).
[45] B. Fang, O. Cohen, and V. O. Lorenz, J. Opt. Soc. Am. B **31**, 277 (2014).
[46] U. Leonhardt, Phys. Rev. A **48**, 3265 (1993).
[47] K. Kreis, arXiv:1211.2880.
[48] M. M. Wolf and D. Perez-Garcia, Phys. Rev. A **75**, 012303 (2007).
[49] S. J. van Enk and O. Hirota, Phys. Rev. A **64**, 022313 (2001).
[50] X. Wang, J. Phys. A: Math. Gen. **35**, 165 (2001).
[51] M. F. Santos, P. Milman, L. Davidovich, and N. Zagury, Phys. Rev. A **73**, 040305(R) (2006).
[52] O. Morin, J.-D. Bancal, M. Ho, P. Sekatski, V. D'Auria, N. Gisin, J. Laurat, and N. Sangouard, Phys. Rev. Lett. **110**, 130401 (2013).
[53] B. Qi, P. Lougovski, and B. P. Williams, Opt. Express **28**, 2276 (2020).
[54] H. Le Jeannic, Theses, Université Pierre et Marie Curie, Paris VI, 2016.
[55] K. Laiho, M. Avenhaus, K. Cassemiro, and C. Silberhorn, New J. Phys. **11**, 043012 (2009).
[56] N. Sridhar, R. Shahrokhshahi, A. J. Miller, B. Calkins, T. Gerrits, A. Lita, S. W. Nam, and O. Pfister, J. Opt. Soc. Am. B **31**, B34 (2014).
[57] U. Chabaud, T. Douce, F. Grosshans, E. Kashefi, D. Markham, *Building Trust for Continuous Variable Quantum States*, Leibniz International Proceedings in Informatics (LIPIcs), Vol. 158 (Schloss Dagstuhl-Leibniz-Zentrum fur Informatik, Dagstuhl, Germany, 2020), pp. 3:1–3:15.